1661-8726/08/010223–13
DOI 10.1007/s00015-008-1249-1
Birkhäuser Verlag, Basel, 2008

Swiss J. Geosci. 101 (2008) 223–235

Composite faults in the Swiss Alps formed by the interplay of tectonics, gravitation and postglacial rebound: an integrated field and modelling study

Michaela E. Ustaszewski[1,*], Andrea Hampel[2] & O. Adrian Pfiffner[1]

Key words: active faults, gravitational movements, uphill-facing scarps, numerical modelling, post-glacial differential uplift, Swiss Alps

ABSTRACT

Along the flanks of several valleys in the Swiss Alps, well-preserved fault scarps occur between 1900 and 2400 m altitude, which reveal uplift of the valley-side block relative to the mountain-side block. The height of these uphill-facing scarps varies between 0.5 m and more than 10 m along strike of the fault traces, which usually trend parallel to the valley axes. The formation of the scarps is generally attributed either to tectonic movements or gravitational slope instabilities. Here we combine field data and numerical experiments to show that the scarps may be of composite origin, i.e. that tectonic and gravitational processes as well as postglacial differential uplift may have contributed to their formation. Tectonic displacement may occur as the fault scarps run parallel to older tectonic faults. The tectonic component seems, however, to be minor as the studied valleys lack seismic activity. A large gravitational component, which is feasible owing to the steep dip of the schistosity and lithologic boundaries in the studied valleys, is indicated by the uneven morphology of the scarps, which is typical of slope movements. Postglacial differential uplift of the valley floor with respect to the summits provides a third feasible mechanism for scarp formation, as the scarps are postglacial in age and occur on the flanks of valleys that were filled with ice during the last glacial maximum. Finite-element experiments show that postglacial unloading and rebound can initiate slip on steeply dipping pre-existing weak zones and explain part of the observed scarp height. From our field and modelling results we conclude that the formation of uphill-facing scarps is primarily promoted by a steeply dipping schistosity striking parallel to the valley axes and, in addition, by mechanically weaker rocks in the valley with respect to the summits. Our findings imply that the identification of surface expressions related to active faults can be hindered by similar morphologic structures of non-tectonic origin.

Introduction

Mountain belts like the Himalayas or the European Alps form owing to the collision of two continental plates (e.g. Molnar & Tapponnier 1975; Schmid et al. 1996). The total amount of convergence between the two plates is usually accommodated by many faults, each of which slips at a lower rate than the total convergence velocity (e.g. Bilham et al. 1997; Wang et al. 2001). Identification of active faults and determination of neotectonic displacements is crucial to decipher the current deformation pattern within a mountain belt and, ultimately, to estimate the seismic potential of different regions (Tapponnier & Molnar 1979; van der Woerd et al. 2001; Hetzel et al. 2004; Persaud & Pfiffner 2004). The identification of active tectonic faults may, however, be hindered by non-tectonic processes like gravitational slope movements that have morphologic characteristics similar to the surface expression of active tectonic faults.

A particular class of such morphologic structures that may or may not have a tectonic origin are uphill-facing scarps (also called antislope, counter, or antithetic scarps). They typically occur along the flanks of valleys and form by uplift of the valley-side block relative to the mountain-side block. Uphill-facing scarps have been reported from many mountain ranges, e.g., the Rocky Mountains (McCalpin & Irvine 1995), the Coast Mountains of British Columbia (Bovis 1982), Alaska (Radbruch-Hall 1978), the Northern Carpathian Mountains (Mahr & Nemcok 1977), the Pyrenees (Gutiérrez-Santolalla et al. 2005) and in Scotland (Jarmann 2006). They were earlier described in the European Alps (Jäckli 1951, 1965) and extensively studied by numerous workers (e.g. Renner 1982; Eckardt et al. 1983; Agliardi et al. 2001; Persaud & Pfiffner 2004; Amann 2005; Hippolyte et al. 2006; Jomard 2006). The formation of the scarps has been attributed to different mechanisms, which can be summarized as gravitational slope deformation (Hippolyte et al. 2006; Gutiérrez-Santolalla et al. 2005), neotectonic fault-

[1] Institute of Geological Sciences, University of Bern, Baltzerstrasse 1–3, 3012 Bern, Switzerland.
[2] Institute of Geology, Mineralogy and Geophysics, Ruhr-University Bochum, Universitätsstrasse 150, 44801 Bochum, Germany.
*Corresponding author: M. Ustaszewski. E-mail: michaela@ntu.edu.tw, now at: Department of Geosciences, National Taiwan University. No. 1, Sec. 4, Roosevelt Road, Taipei 10617, Taiwan.

ing (Eckhardt et al. 1983; Persaud & Pfiffner 2004) or differential postglacial uplift (Jäckli 1965; Jarman 2006). Which of the proposed mechanisms is definitely responsible for scarp formation is still not fully resolved.

Here we present results from a field study in the central Swiss Alps, where the abundant occurrence of uphill-facing scarps provides an ideal opportunity to explore their characteristics and formation mechanisms. In addition to the field study, we performed finite-element experiments to test if the scarps, which developed in formerly glaciated valleys, may be caused by postglacial rebound. The aim of this study was to investigate, if all three processes in question – differential postglacial uplift, gravitational slope movement and, to a minor extent, crustal deformation – contributed to the formation of the uphill-facing scarps.

Geological setting and field observations

In the central Swiss Alps, faults with uphill-facing scarps cluster mainly between 1900 and 2400 m altitude along valley flanks of the Upper Rhone valley, the Urseren valley, the Upper Rhine valley, and along the Bedretto valley (Fig. 1; e.g. Eckardt et al. 1983; Ustaszewski 2007; Ustaszewski & Pfiffner 2008). In the Upper Rhone valley, the Urseren valley, the Upper Rhine valley, faults occur over a distance of ~90 km between the towns Brig and Trun, whereas in the Bedretto valley they are present over a distance of ~10 km. The length of the individual faults varies between a few hundreds of meters to 7 km. The faults strike predominantly parallel to the valley and are characterized by linear surface traces, indicating vertical faults. They tend to follow pre-existing geological structures like lamprophyric dykes (Keller & Schneider 1982; Amann 2005), lithologic

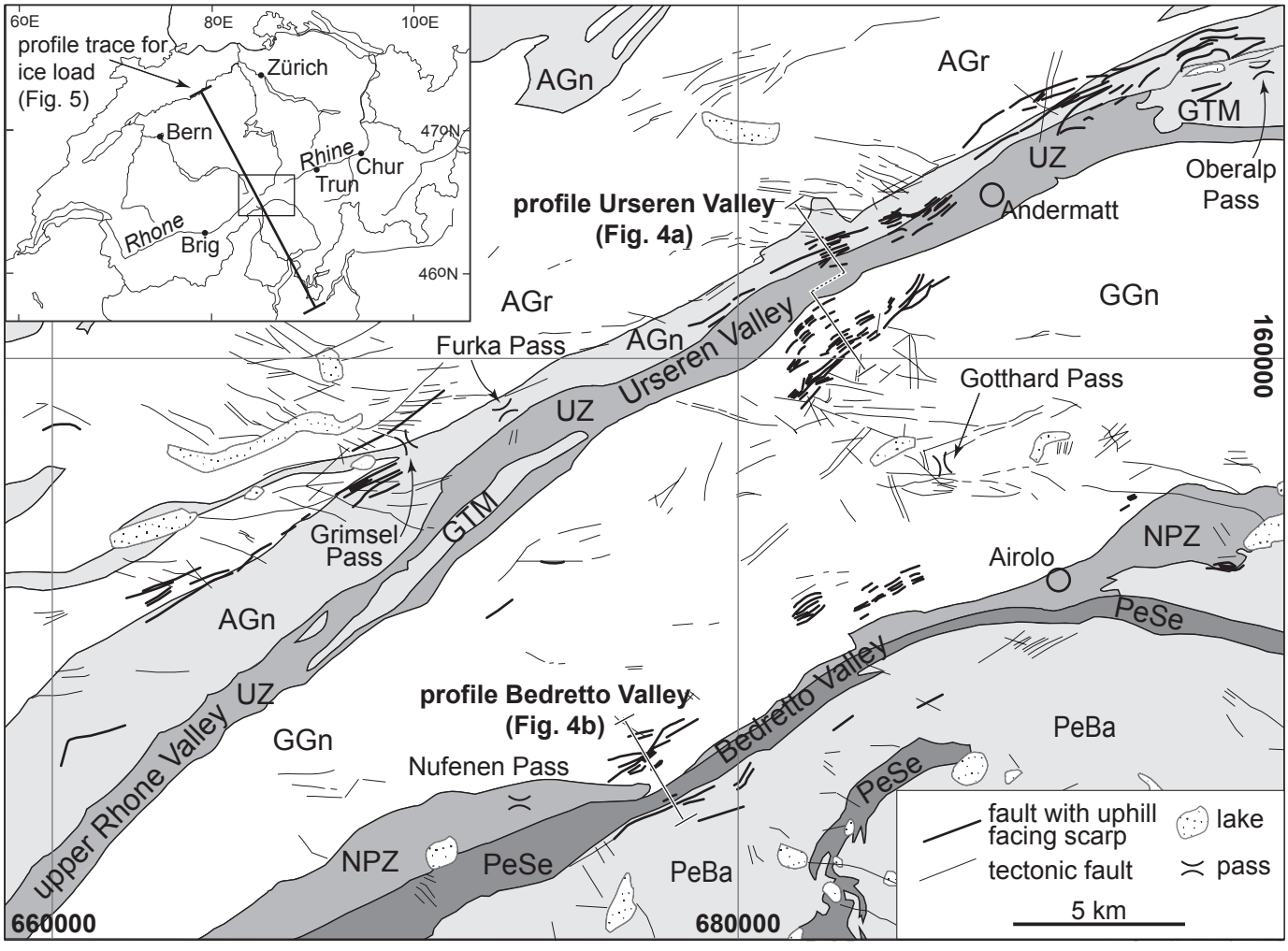

Fig. 1. Tectonic map of the study area. Tectonic faults and faults with uphill-facing scarps mapped from aerial photographs and identified by fieldwork are indicated by thin and thick solid lines, respectively. The geological profiles of Fig. 4 are marked on the tectonic map. The profile, along which the ice load for the finite-element model (Fig. 5) is estimated, is shown on the inset map. AGn – Aar Gneiss; AGr – Aar Granite; UZ – Urseren Zone; GTM – Goms/Tavetsch Massif (gneiss); GGn – Gotthard Granites and Gneisses; NPZ – mesozoic cover sediments including Nufenen and Piora Zone; PeSe – Penninic sediment nappes; PeBa – Penninic basement nappes;

boundaries, foliation (Fig. 2a) and fault zones. The faults occur – from north to south – in the following tectonic units (Figs. 1 and 4): the Aar massif with the central Aar granite and southern gneiss zone, the Urseren zone (Mesozoic metasediments) in the Urseren valley, the Gotthard massif with granites and gneisses, the Nufenen zone (Mesozoic metasediments) in the Bedretto valley, and schists and gneisses of Penninic sediment and basement nappes. Schistosity is predominantly vertical and parallel to the valley-axes, striking SW–NE to WSW–ENE.

The uphill-facing scarps related to the observed faults occur on both flanks of the valleys and show a pronounced morphology. Where bedrock scarps are vertical or steeply inclined towards the mountain ridge they are often exposed and look fresh. No indicators of slip directions were found on the fault scarps. Some scarps are partly to completely covered by slope talus and/or vegetation (Fig. 2b). In the depression behind the fault, slope talus and debris have accumulated. This material often seals the base of the depression and water loggings and small lakes are dammed by the uphill-facing scarp (Figs. 2b, c, g). The height of the scarps varies from 50 cm to more than 10 m, although even higher offsets may be plausible as debris in the depressions behind the faults covers the lower part of the scarp. Note that the scarp height varies along strike of the fault (see Figs. 2d–e). Within 100 m distance, the offset can change from 0.5 to 10 meters. The highest displacements occur where the scarp-related fault crosses a ridge on a valley flank, and they are smallest where the fault transects a side-valley.

The depth extent of the scarp-related faults can be derived from observations made by Furrer (1948) and Keller & Schneider (1982). Furrer (1948) reports extensive water inleakage during the excavation of the Riederhorn gallery at the Riederalp (Upper Rhone valley, ~6 km NE of Brig). On the Riederalp, a dense array of faults with uphill-facing scarps occurs, and deep-reaching toppling phenomena can be observed along the valley flank. The building of the Riederhorn gallery led to a severe ebbing of numerous springs in the area above the gallery. Furrer explains that the springs were joint-related overflow springs and the penetration of the joints by the gallery caused their drainage. This implies that these joints, which we relate to the scarp-associated faults, are open to a depth of at least 700 m. Keller & Schneider (1982), who report geotechnical problems during excavation of the Bedretto tunnel caused by toppling phenomena, derive a base plane of the toppling, which reaches 150 to 200 m below today's valley floor. They explain the position of the base plane due to glacial over-deepening of the Bedretto valley and enhanced erosion of evaporitic sediments of the Nufenen Zone at the valley floor, which both created space for the mass movements. The toppling observed in the tunnel is linked to the uphill-facing scarps on the surface above the tunnel (Keller & Schneider, 1982).

The age of the fault scarps is constrained to be postglacial because they offset moraines and slope talus (Figs. 2c–d). Interestingly, Jäckli (1951) and Renner (1982) reported larger offsets of older, Daun-stage moraines (Older Dryas stadial, ~12'000 ^{14}C yr BP; Preusser, 2004) than of younger, Egesen-stage moraines (Younger Dryas stadial, ~10'000 ^{14}C yr BP; Preusser, 2004). This indicates that the faults accumulated more slip before ~11'000 years than afterwards. Furthermore, the scarps occur in areas that were heavily glaciated during the Last Glacial Maximum. As the glaciers eroded deeply into the bedrock and polished the rock surfaces (Kelly et al. 2006; Ivy-Ochs et al. 2007; Benn & Evans 1998), it seems unlikely that the scarps should survive these abrasive processes.

After their formation, some uphill-facing scarps have been cut by recent fast gravitational movements like debris flows (Fig. 2f), which partly erode the scarps. In the Urseren and Bedretto valleys, the valley flanks are also affected by slow deep-seated gravitational slope deformations. This can be observed by antithetic faults dipping towards the mountain flank (Figs. 3a–b), counter scarps and associated troughs, extension joints, and toppling phenomena (Fig. 3c, d). In the study area, flexural toppling prevails, because rocks are intensely foliated forming narrow packages of gneiss or schist. Only in few locations, mainly in less densely foliated gneisses, block toppling is observed. The uneven topography of the valley flanks and the scarps with pronounced along-strike variations in their height resemble the morphologic expressions caused by large-scale sagging processes and the accompanying smaller-scale gravitational processes (Agliardi et al. 2001; Dramis & Sorriso-Valvo 1994; Gutiérrez-Santolalla et al. 2005 and references therein; Hippolyte et al. 2006; Madritsch & Millen 2007). At least some of the scarp-related faults are still active: At the Oberalp Pass, geodetic measurements along a ~170-m-long profile reveal height changes of ~0.7 mm/yr across a fault with an uphill-facing scarp (Eckhardt et al. 1983).

In summary, the valleys with uphill-facing scarps have the following characteristics in common. First, they are characterized by similar geology, with granite gneisses in the summit areas (except the southern side of the Bedretto valley), schists and gneisses along the valley shoulders and Triassic metamorphic sediments at the valley floor (Fig. 4). The scarp-related faults usually parallel pre-existing structures and may be reactivated older tectonic faults. Second, the predominant schistosity in all valleys is vertical and parallel to the valley axes. Third, the scarps are of postglacial age and share a similar glacial history, i.e. all valleys, in which uphill-facing scarps developed, were located beneath large ice domes during the Last Glacial Maximum (Florineth & Schlüchter 1998; Kelly et al. 2004). These ice domes started to form about 35'000 years ago (e.g. Ivy-Ochs et al. 2006).

Numerical Modelling

The postglacial age of the scarps suggests a relationship between their formation and the deglaciation of the valleys. As Jäckli (1965) proposed, deglaciation might have lead to differential uplift of the valley floor with respect to the summits. Calculations by Gudmundsson (1994) and Barletta et al. (2006) indeed showed that melting of the glaciers in Switzerland induced rebound and uplift. Persaud & Pfiffner (2004) analyzed

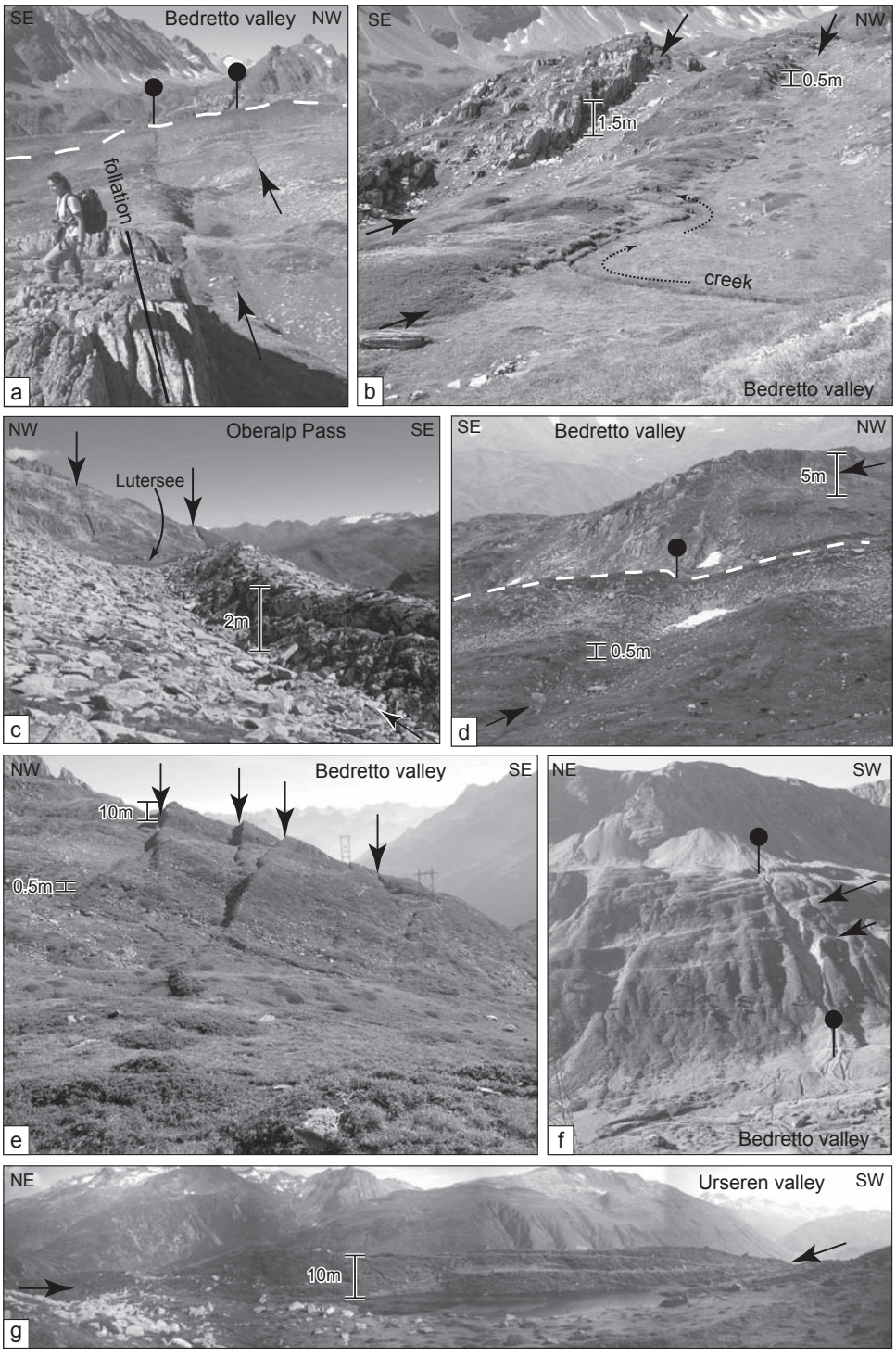

Fig. 2 Field photographs: arrows indicate faults with uphill facing scarps, pins indicate cross-cutting relationships. a) Uphill facing scarp in the Bedretto valley dissecting a moraine ridge (stippled white line) and paralleling the foliation of the gneisses. b) A morphologically pronounced uphill facing scarp in the SE and a weaker expressed uphill facing scarp in the NW with both uphill-facing scarps and surface displacements of 1.5 m and 0.5 m, respectively, situated on the Alpe di Manio in the Bedretto valley. A small creek (dotted line) is diverted by the scarp. c) Pronounced uphill-facing scarp at the Lutersee near the Oberalp Pass, displacing slope talus by ~2 m. The Lutersee in the background is dammed by the uphill-facing scarp. d) Fault with pronounced uphill-facing scarp and varying displacement along-strike (from ~5 m in the background to ~0.5 m in the foreground) on the Alpe die Manio in the Bedretto valley. The fault displaces a moraine ridge (stippled white line) by ~1.5 m. e) Faults in the Bedretto valley with substantial displacement variation along-strike (from ~10 m in the background to ~0.5 m in the foreground). f) Faults with uphill-facing scarps on the southern slope of the Bedretto valley are dissected by debris flow channels. g) Pronounced uphill-facing scarps NW of Andermatt in the Urseren valley. The height of the largest scarp is about 10 m and dams a small lake.

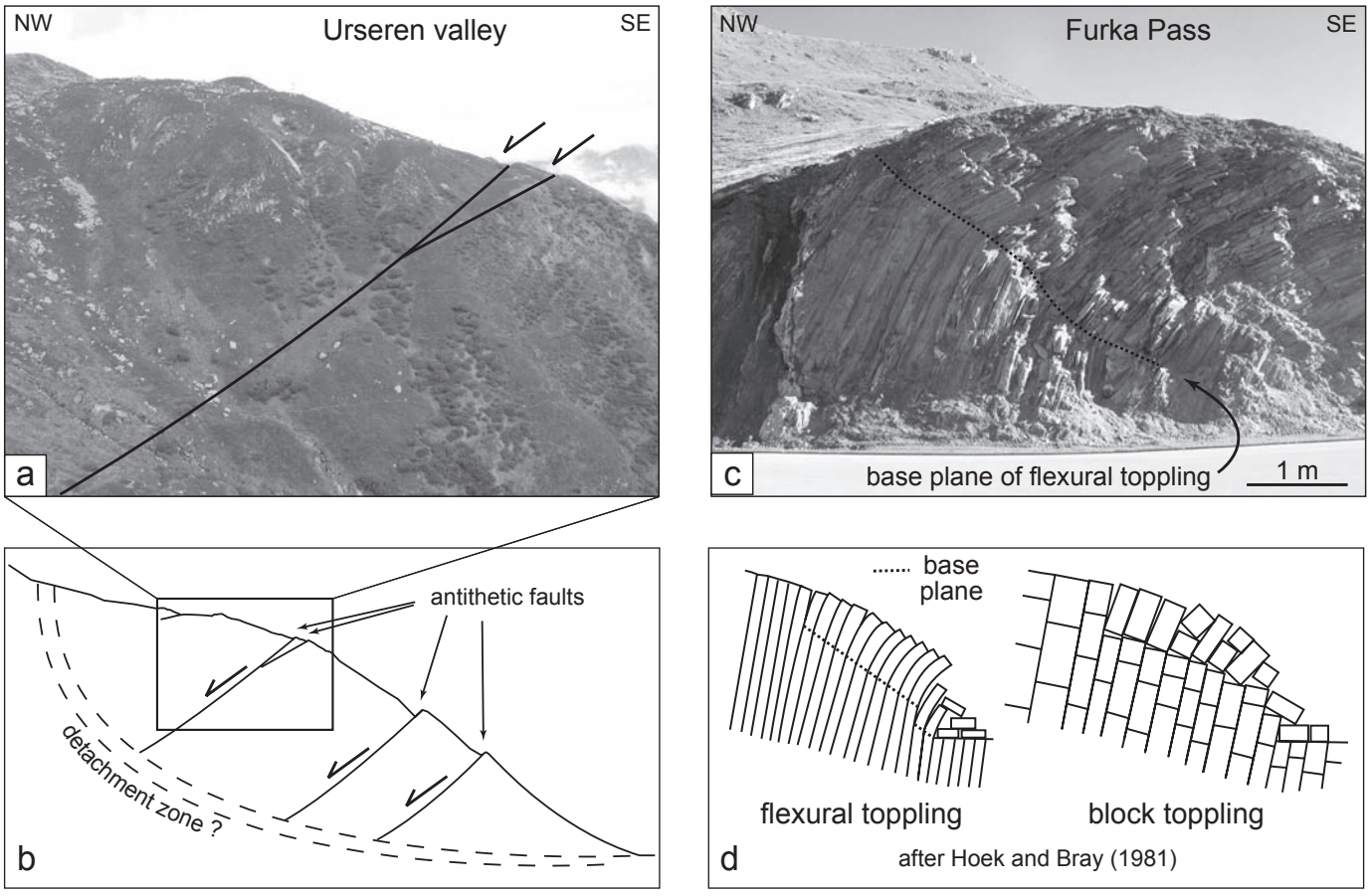

Fig. 3. Gravitational processes at the valley flanks. a) Antithetic faults with uphill facing scarps in the Urseren valley dip towards a possible detachment zone of a deep-seated gravitational slope movement. b) Schematic sketch of a deep-seated gravitational slope deformation. c) Toppling of the steeply foliated Aar Gneiss at the Furka Pass. d) Different types of toppling after Hoek & Bray (1981).

the effect of an ice load and the postglacial rebound using a numerical model, in which the lithosphere of the Alps is represented by a continuous plate of equivalent elastic thickness. Their model does not include individual faults and predicts an orogen scale uplift pattern that has a wavelength larger than the one observed from present-day uplift (Kahle et al. 1997). The model, however, is not suited to analyze the valley-scale uplift pattern.

Here we apply a different model approach that includes pre-existing fault planes, which may be activated during deglaciation if a critical shear stress is reached, in order to test if uphill-facing scarps may be caused by postglacial unloading and rebound. The model setup is inspired by the observation that re-activation of pre-existing weak zones may play a crucial role in the formation of uphill-facing scarps (Jäckli 1965; Eckardt et al. 1983). Our model setup allows us to calculate both the rebound of the Alps after the Last Glacial Maximum on a lithospheric scale and to investigate the effects of postglacial unloading and rebound on local crustal deformation. Our models are carried out using the commercial software package ABAQUS (Hibbitt et al. 2006).

Setup of the finite-element model

The model represents a 1500-km-long and 100-km-thick lithosphere, which is divided into an elastic upper crust, a viscoelastic lower crust and a viscoelastic lithospheric mantle (Fig. 5a). The rheological properties of the layers (cf. Turcotte & Schubert 2002) are given in Figure 5. Based on a topographic profile (Fig. 4a) the topography of the Urseren valley is included in the centre of the model (Fig. 5). Seven potential slip planes are incorporated into the crust (Fig. 5b): Fault plane 1 represents the contact between the central Aar granite and southern gneiss zone of the Aar massif, whereas fault plane 7 represents the boundary between the northern gneiss zone of the Gotthard massif and the Gotthard ortho-gneiss (Figs. 4–5). To account for the contrast between the metasediments and the Aar granites or Gotthard orthogneisses, respectively, the approximately top 5 km of the region between fault planes 1 and 7 have a lower Young's modulus (grey-shaded area in Fig. 5). Fault planes 2–5 represent the boundaries between different schists or foliation planes. Initiation and subsequent slip on the fault planes, which are defined to a depth of 5 km below the valley floor, is con-

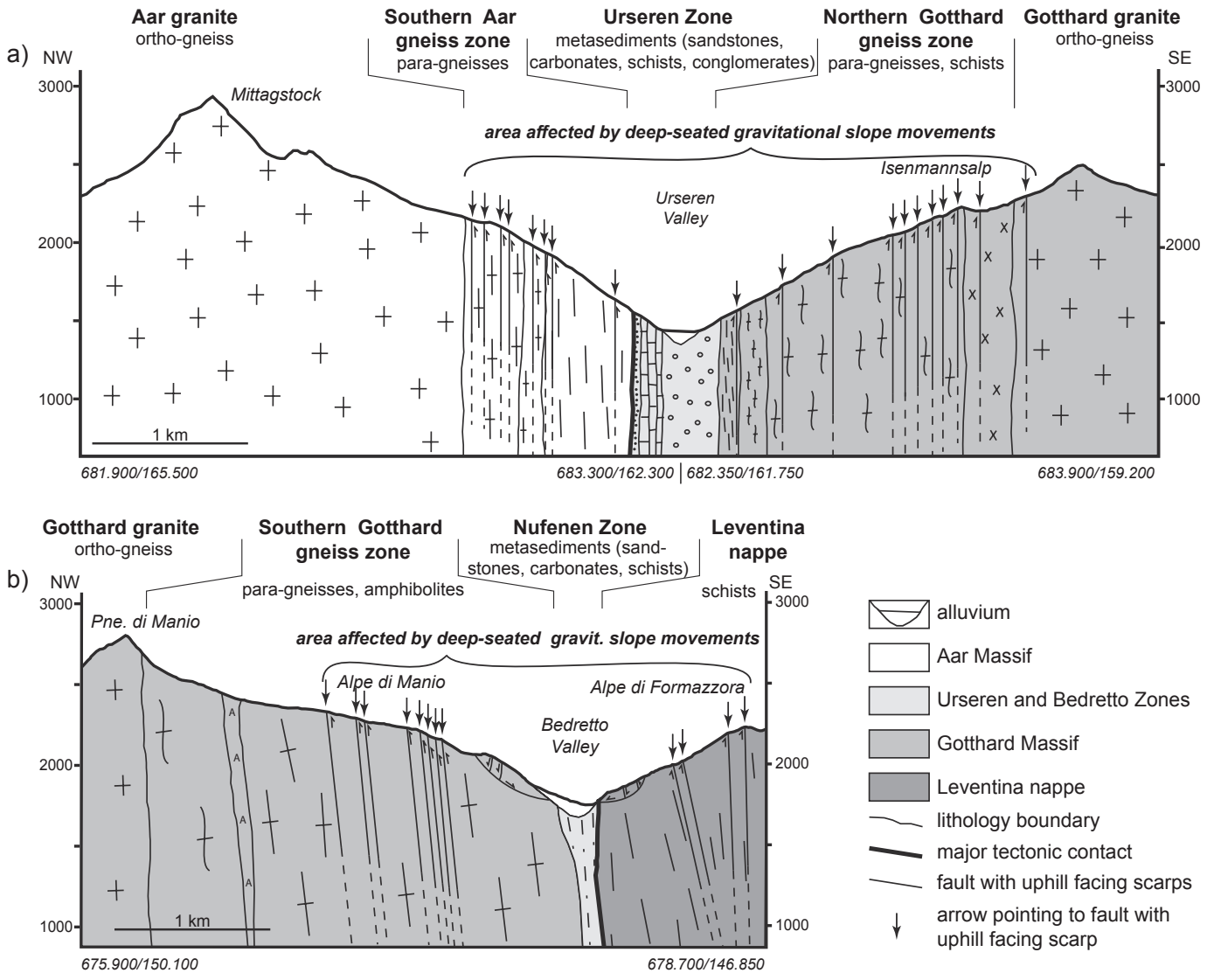

Fig. 4. Geological profiles across a) the Urseren valley and b) the Bedretto valley. Start and end points of profiles specified by coordinates (Swiss National km Grid) and are also given in Fig. 1.

trolled by a Mohr-Coulomb criterion with a friction coefficient of $\mu = 0.4$ and a maximum shear stress of $\tau_{max} = 2 \times 10^6$ Pa (e.g. Weijermars 1997). The latter limits the shear stress that may be reached on the fault planes and reflects their mechanical weakness. Experiments were carried out with vertical (Fig. 5b), 45°-dipping and 22°-dipping fault planes (not shown in Fig. 5). The inclined faults dip away from the valley slope, i.e. the three model faults north of the valley axis dip to the northwest, whereas the four faults south of the valley dip southeastward.

Gravity is included in the model as a body force. We implement isostasy by adding an elastic foundation, which represents the density of the asthenosphere ($\rho_{asth} = 3200$ kg/m^3) and a lithostatic pressure ($P_{litho} = 3.03 \times 10^9$ Pa) at the bottom of the model. The viscosity of the asthenosphere ($\eta_{asth} = 1 \times 10^{19}$ Pa s) is represented by linear dashpot elements at the bottom of the model. At the beginning of each experiment, the model attains isostatic equilibrium. Afterwards, the left and right model sides are fixed in the horizontal and the vertical directions and pressure loads representing the glaciers in the Urseren and neighbouring valleys are applied (Fig. 5a). The magnitude of the ice load in the Urseren valley (Fig. 5b) is calculated from the inferred altitude of the ice surface at 2600 m (Jäckli 1965; Florineth & Schlüchter 1998). In the model we apply a hydrostatic pressure, which linearly increases from zero at 2600 m to a maximum pressure that is equivalent to 1225 m of ice at the valley floor (Fig. 5a). For the regions north and south of the Urseren valley, we average the ice thickness over 25-km-long-segments of a profile running from Aarau to Caccivio (see Fig. 1). The estimated values of the ice thickness along this profile are shown in Figure 5a. The magnitude of the ice load is at a maximum at

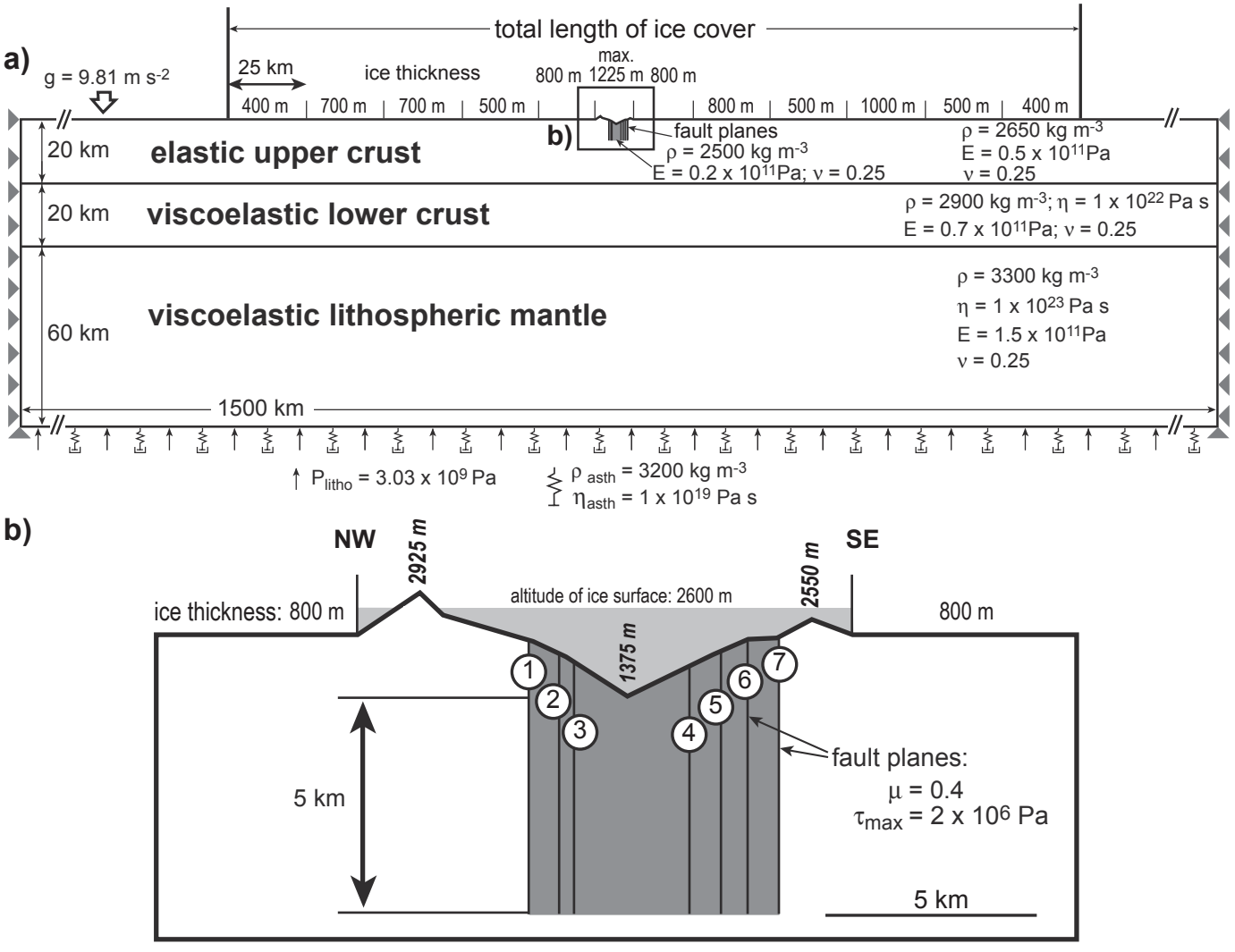

Fig. 5. Setup of the finite-element-model. a) Geometry of the model lithosphere. Box marks the central part of the model, which is shown enlarged in Fig. 5b. The model sides are fixed in the horizontal and vertical direction (grey triangles). The rheological parameters are density (ρ), Young's modulus (E), Poisson's ratio (ν), viscosity (η), acceleration due to gravity (g), and lithostatic pressure (P_{litho}, marked by black arrows at bottom of model). The density and viscosity of the asthenosphere enter the model through spring and dashpot elements at the bottom of the model. b) Enlarged view of the center of the model, which has a topography according to a simplified topographic profile of the Urseren valley. Bold italic numbers indicate altitude of the northern and southern peaks and the valley floor; italic numbers indicate altitude of major scarps in the Urseren valley. Slip on the fault planes (numbered 1–7) is controlled by a Mohr-Coulomb failure criterion (τ_{max}: maximum shear stress of the fault; μ: coefficient of friction).

the beginning of the model run and then decreases linearly to zero within a time span of 1, 3 or 10 ka in different experiments, respectively, to investigate if the rate of deglaciation affects the formation and height of the scarps. We prefer the model with a deglaciation within 3 ka because surface exposure dating of glacial deposits and bedrock surfaces suggests that most glaciers retreated between ~21 ka and ~18 ka BP (Ivy-Ochs et al. 2006).

Results of the finite-element experiments

The first set of experiments is carried out with vertical fault planes. Application of the ice load leads to ~135 m of subsidence in the centre of the model. During presence of the ice, no slip occurs on the fault planes, i.e. the Mohr circle for stress has not yet reached the line of the Mohr-Coulomb criterion at any point on the fault. When the removal of the ice load begins, slip on the fault is initiated, i.e. the Mohr circle touches the line of the Mohr-Coulomb criterion. The scarps that form at the model surface as result of the slip on the fault planes are uphill-facing scarps on both sides of the valley (Fig. 6a). For a deglaciation within 3 ka, maximum scarp heights of 2.46 m and 1.11 m are attained on the northernmost and southernmost fault planes, respectively (Fig. 6a, Table 1). The difference in the scarp height is caused by the asymmetry of the valley. Scarps related to fault planes 2–6 are between 0.5–0.8 m high (Table 1). Faster

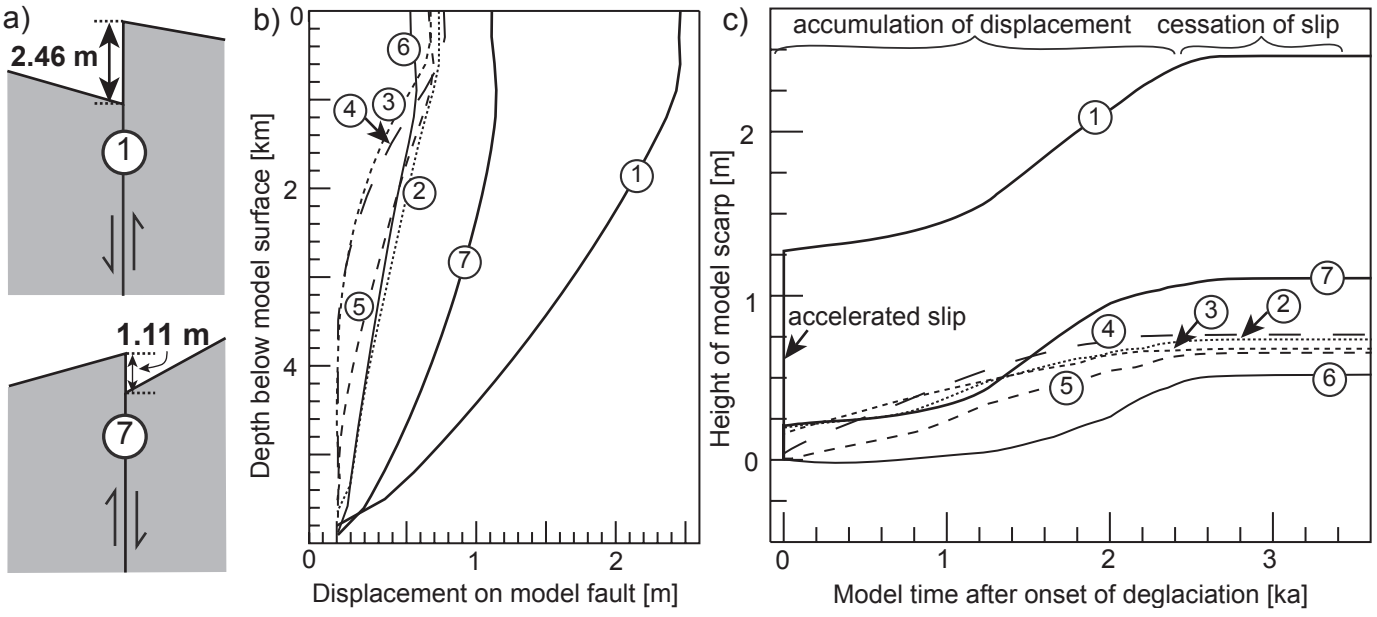

Fig. 6. Results of the model with vertical fault planes and deglaciation within 3 ka. a) Detail sections showing the uphill-facing scarps that develop as a consequence of deglaciation on fault 1 north of the valley axis and fault 7 south of the valley axis. No vertical exaggeration. b) Plot showing the displacement on the fault planes 1–7 versus depth below model surface. c) Evolution of fault slip at the surface. Numbers refer to the fault planes shown in Figure 5b.

deglaciation within 1 ka leads to slightly higher scarp heights, whereas unloading within 10 ka only slightly decreases the final scarp heights (Table 1). The displacement on the faults is largest to a depth of 1 km below the surface and decreases beneath this depth (Fig. 6b). As the temporal slip evolution in Figure 6c shows, the slip rates on the individual faults vary considerably until the final total displacements are achieved. At the onset of the deglaciation, the outermost faults (faults 1 and 7) experience a short phase of rapid motion, which is followed by a longer time interval during which slip accumulation almost ceases. Afterwards, slip continues at a constant rate before it ceases again near the end of the deglaciation (Fig. 6c). These three phases in the evolution – enhanced slip at the onset of deglaciation followed by a phase during which most slip is accumulated and finally cessation of slip at the end of unloading – occur in all experiments irrespectively of the deglaciation rate. Faults 2–6 lack the incipient phase with rapid slip and partly also the first phase of slip cessation (Fig. 6c).

In case of 45°-dipping fault planes, unloading of the model within 3 ka causes slip only on the northernmost and southernmost fault planes (no. 1, 7), where uphill-facing scarps of 1.01 m and 0.28 m height develop (Table 1). Again, a shorter unloading phase slightly increases the scarp height, whereas a longer unloading phase decreases it. On both fault planes, the total displacement at the surface is ~1.5 m less than in the experiments with vertical fault planes. When the fault planes have a shallow dip of 22°, no slip occurs on the faults (Table 1).

To evaluate how the rheological properties of the rocks in the valley influence scarp formation, we used the setup with vertical fault planes and a deglaciation within 3 ka and varied the Young's modulus in the region between the faults 1 and 7 (Fig. 5b). If the Young's modulus is the same in the entire upper crust ($E = 0.5 \times 10^{11}$ Pa), all faults still show uphill-facing scarps but the displacements are lower than in the first experiment. For example, faults 1 and 7 show scarp heights of 1.29 m and 0.52 m, respectively. Decreasing the Young's modulus to $E = 0.4 \times 10^{11}$ Pa (and in a second run to $E = 0.3 \times 10^{11}$ Pa) in the region between faults 1 and 7, i.e. to lower values than in the neighbouring upper crust, increases the scarp heights on

Table 1. Numerical modelling results showing the scarp heights at faults 1–7 for different rates of deglaciation. For location and numbering of fault planes see Figure 5.

	height of scarp (*total displacement*) [m] after deglaciation in		
vertical fault planes	**1 ka**	**3 ka**	**10 ka**
1	2.55	2.46	2.46
2	0.76	0.73	0.73
3	0.67	0.67	0.68
4	0.79	0.76	0.75
5	0.69	0.65	0.64
6	0.53	0.52	0.51
7	1.18	1.11	1.10
45°-dipping fault planes	**1 ka**	**3 ka**	**10 ka**
1	1.01 (*1.43*)	0.94 (*1.33*)	0.90 (*1.27*)
2–6	0	0	0
7	0.28 (*0.40*)	0.21 (*0.29*)	0.15 (*0.21*)
22°-dipping fault planes	**1 ka**	**3 ka**	**10 ka**
1–7	0	0	0

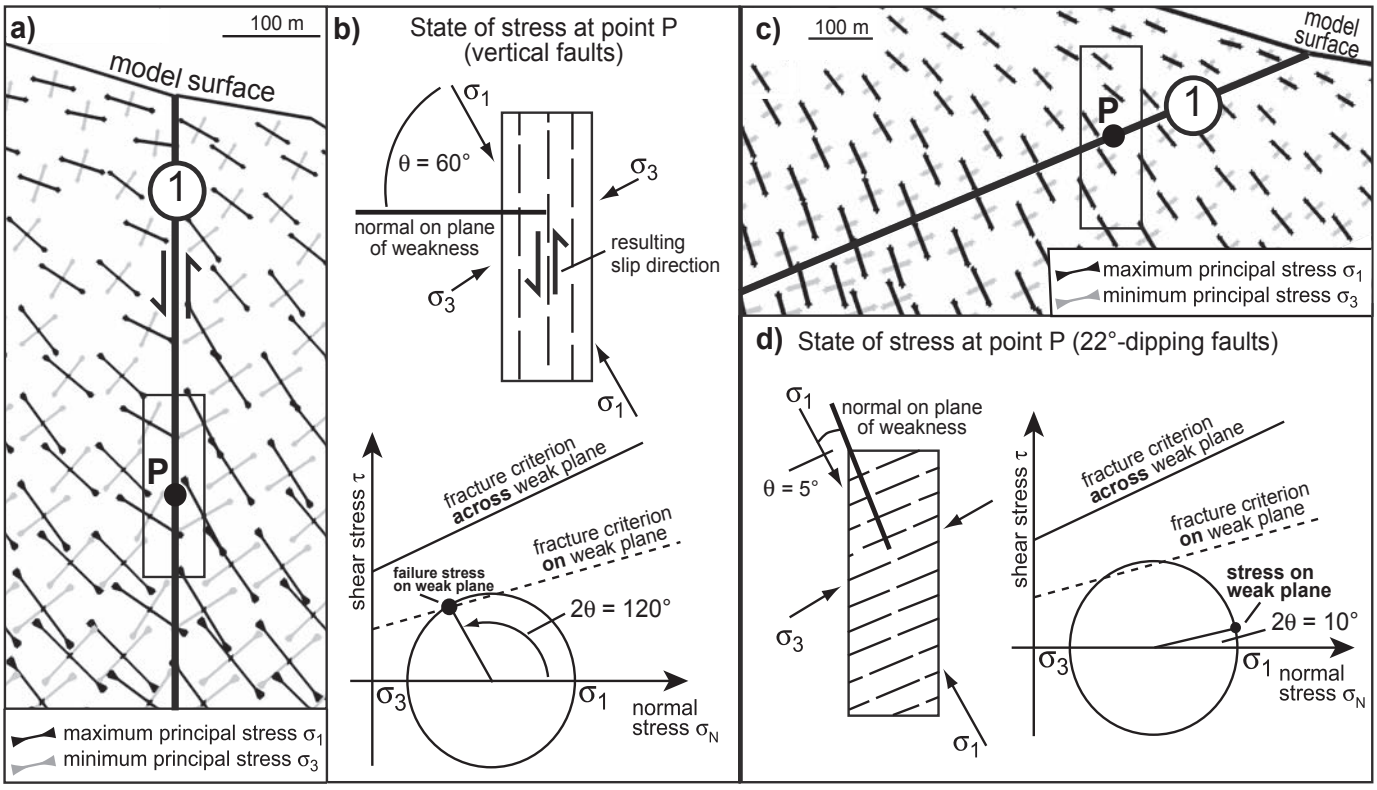

Fig. 7. a) Enlarged section of the model showing the orientation of the maximum and minimum principal compressive stresses σ_1 and σ_3 near the vertical model fault 1. No vertical exaggeration. b) State of stress at P in physical space (upper row) and Mohr space (lower row). The vertical anisotropy of the rock (upper row) represents the mechanically weak planes formed by vertical lithologic boundaries and schistosity. The angle θ between σ_1 and the normal on the weak plane is 60°. In the Mohr diagram, the orientation of the weak plane is given by the angle $2\theta = 120°$ (black dot on Mohr circle). The two fracture criteria illustrate that the critical shear stress for slip *across* the weak plane (solid line) is larger than the shear stress required for slip *on* the weak plane (dashed line). Slip *on* the weak plane occurs because its orientation is such that the Mohr circle touches the fracture criterion (dashed line), i.e. the critical shear stress on the weak plane is reached. c) Modelled orientation of σ_1 and σ_3 near fault 1 dipping 22°. d) State of stress at P in physical space (left) and Mohr space (right). The angle θ between σ_1 and the normal on the weak plane is 5°. The Mohr diagram shows that the shear stress on the fault plane with an orientation of $2\theta = 10°$ is lower than the critical shear stress and thus no slip occurs on the fault.

faults 1 and 7 to 1.60 m (1.93 m) and 0.65 m (0.93 m), respectively.

Discussion

Our field observations and numerical experiments reveal that steeply dipping weak zones are a necessary pre-requisite for the formation of uphill-facing scarps. These weak zones may be defined by older faults, lithologic boundaries or schistosity. In contrast, shallow-dipping discontinuities inhibit the formation of uphill-facings scarps, which agrees with the observation that valleys incised in rocks with shallow dipping foliation (e.g. Prättigau, Rhone Valley downstream of Leuk, Rhine Valley downstream of Ilanz, Val d'Hérens) consistently lack uphill-facing scarps. Weaker mechanical properties (a lower Young's modulus) of the rocks in the valley compared to the ridges additionally promote scarp formation in the model. This agrees with the field observation that the valleys with uphill-facing scarps consist of pervasively foliated metasediments, which are mechanically weaker than the granites and gneisses comprising the ridges.

The difference in the behaviour of vertical and shallow-dipping fault planes during unloading is readily explained by the different orientation of the principal stresses with respect to the zones of weakness (e.g. Twiss & Moores 2007, page 221–224). In case of a vertical fault plane, the maximum principal stress σ_1 is oriented at an angle of ~30° to the fault (Fig. 7a; applied sign convention: compression positive). To analyse the state of stress at point P (Fig. 7a), the orientation of the principal stresses is plotted in physical space for a rock with vertical planes of weakness (Fig. 7b). The angle θ between σ_1 and the normal on the plane of weakness is 60° (Fig. 7b). In the Mohr diagram, the anisotropy of the rock is represented by two fracture criteria, which take into account that the strength on the plane of weakness is lower than across the plane of weakness (Fig. 7b). For a vertical fault plane and $\theta = 60°$, which becomes $2\theta = 120°$ in Mohr space (black dot on Mohr circle), the shear stress on the weak plane reaches the critical shear stress de-

fined by the fracture criterion for the weak plane (Fig. 7b). The resulting slip direction leads to uplift of the valley-side block and hence to the formation of an uphill-facing scarp (Fig. 7b). Thereby, faults 1 and 7 show the fastest slip initiation and the largest displacement because they are optimally oriented with respect to σ_1, whereas σ_1 is inclined slightly steeper around faults 2–6. In contrast, σ_1 is approximately perpendicular to a 22°-dipping fault at point P (Fig. 7c), i.e. the normal on the plane of weakness forms an angle of $\theta = 5°$ with σ_1 (Fig. 7c). As the Mohr diagram shows, the shear stress on the plane of weakness is below the critical shear stress for the weak plane. Thus, no slip occurs on the shallow-dipping fault plane.

With respect to the formation mechanisms, we infer that uphill-facing scarps develop owing to the combined effect of gravitational slope movements as observed in the field, postglacial differential uplift derived from the models, and crustal deformation suggested by the tectonic setting (Fig. 8). We therefore propose the term "composite" fault for these structures. In contrast, most previous workers explained the formation of uphill facing scarps either by gravitational movements only (e.g. Hippolyte et al. 2006) or speculated about post-glacial rebound as the driving mechanism (e.g. Jäckli, 1965). In this study, it could be shown for the first time that post-glacial rebound can cause uphill-facing scarps in the Swiss Alps. Our approach combines the different interpretations and emphasizes the composite origin of these faults due to gravitational movements, post-glacial rebound and crustal deformation.

Depending on the local setting, the three mechanisms may be of different relative importance for the evolution of an individual composite fault. In the central Swiss Alps, postglacial unloading and rebound played a major role for the slip initiation on the composite faults as suggested by the numerical experiments. Furthermore, our models show that postglacial differential uplift as proposed by Jäckli (1965) indeed provides a feasible mechanism for the formation of uphill-facing scarps. Repeated re-activation of the steeply dipping weak zones after the earlier glaciations of the Alps may have induced their further weakening. The modelled slip accumulation during deglaciation is in accordance with the observation that a considerable portion of the displacement on the faults occurred prior to the Egesen-stage in the Alps. Our results imply that deglaciation of the Alps did not only lead to uplift as shown by Gudmundsson (1994) and Persaud & Pfiffner (2004), but also affected faulting by changing the stress in the upper crust. Such a causal relationship between deglaciation, rebound and faulting has long been inferred for other regions that experienced postglacial unloading, for example, Scandinavia (Arvidsson 1996; Stewart et al. 2000) and North America (Adams 1989; Sauber et al. 2000). As numerical models without faults showed, the stress changes induced by postglacial unloading and rebound are sufficient to induce faulting (e.g. Johnston et al., 1998). Recent models that explicitly included a fault quantify the variations in the fault slip rate caused by glacial-interglacial changes in surface loads (Hetzel & Hampel 2005; Hampel & Hetzel 2006).

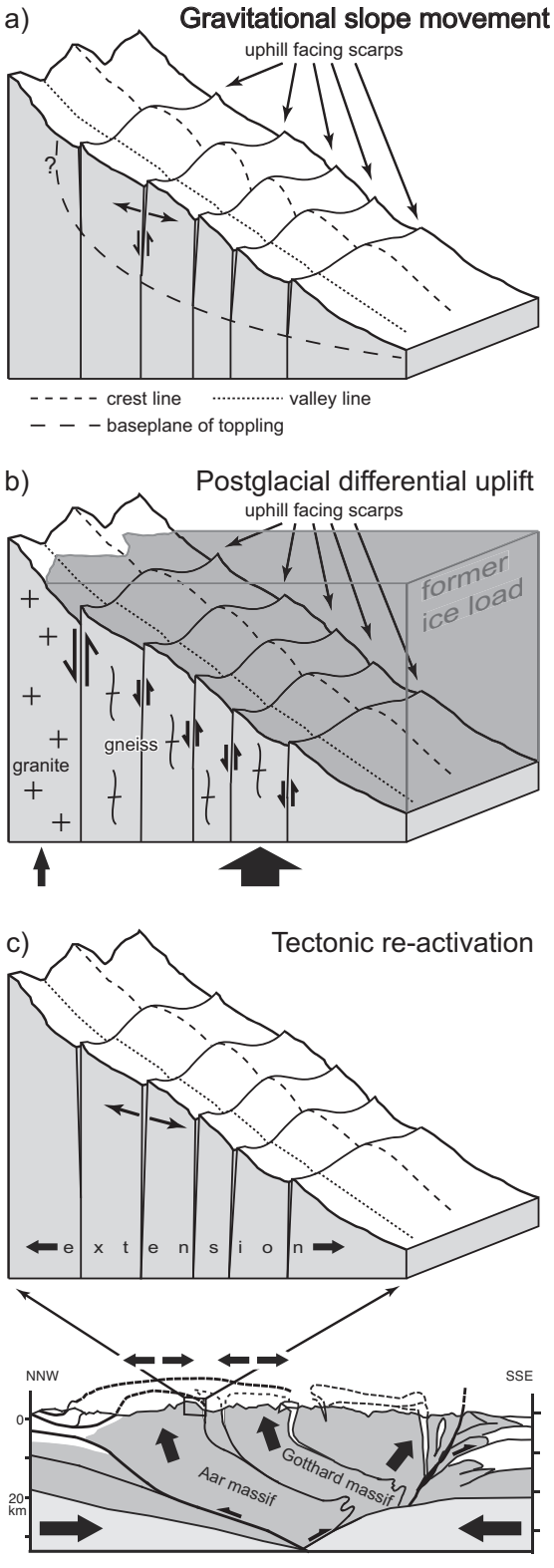

Fig. 8. Schematic block diagrams illustrating a) gravitational reactivation of pre-existing weak zones, b) differential uplift during deglaciation and c) tectonic reactivation in the framework of crustal structure and ongoing convergence. Crest and valley lines highlight the different displacements at crests and valleys due to gravitational movements.

As field observations show, fault slip owing to postglacial unloading can, however, not account for the total displacement on the faults as the modelled maximum scarp height in our experiments is one order of magnitude smaller than the observed maximum displacement in the field (Table 1). Based on our field observations, we attribute most of the additional displacement to gravitational slope movements like large-scale sackung (Fig. 3a) and toppling (Fig. 3b) because these processes can explain the large variations of the scarp height along strike of the composite faults. As suggested by three-dimensional physical models, deep-seated landslides provide a feasible mechanism for the formation of uphill-facing scarps (Bachmann et al. 2004). Furthermore, the observation that displacements are largest when the fault crosses a ridge on the valley flank agrees with the fact that toppling mechanisms act most strongly on the bedrock at ridges (Fig. 8a). Gravitational slip might contribute up to several meters to the total displacement. For example, at the Oberalp Pass, a rough estimate of 7 m can be derived for the gravitational slip during the last 10 ka using recent slip rates of a fault (Eckhardt et al. 1983). Note, however, that gravitational slope movements might not have a constant long-term slip rate, because they are influenced by climate, e.g. periods of strong rainfall or snow melt (Brückl & Parotidis 2005; Sartori et al. 2003).

In contrast to slip by gravitational slope movements, the tectonic component on the composite faults seems to be minor, which agrees with the low recent seismicity (e.g. Baer et al. 1997; Deichmann et al. 2004, 2006) and negligible uplift of the study area (Kahle et al. 1997). Some composite faults in the Upper Rhone Valley, which are associated with joints that are open to a depth of over 700 m (Furrer 1948), could be related to extension in the uppermost part of the orogen. Two mechanisms are feasible to explain this extension. (1) As Selzer (2006) and Selzer et al. (2008) show, basal accretion and associated uplift of crustal flakes in the core of a growing orogen lead to horizontal extension parallel to the convergence direction in the uppermost part. (2) Bulging of the Aar massif basement block is associated with subhorizontal extension at the basement-cover contact (Kammer 1985). Ongoing convergence in the Alps – even if in a waning stage – could thus be held responsible for the observed extension.

Postglacial differential uplift might have contributed to the formation of uphill-facing scarps also in other regions, for example, the Rocky Mountains, the Pyrenees, Scotland or the Argentera Mercantour Massif in southeastern France (Radbruch-Hall 1978; Flageollet 1989; Gutiérrez-Santolalla et al. 2005; Jarman 2006; Jomard 2006). Similar to the Swiss Alps, the scarps in these regions occur on the flanks of formerly glaciated valleys and strike parallel to the valley axes. Most of these authors have so far inferred gravitation as formation mechanism of the uphill facing scarps in these regions, partly triggered by the destabilization of over-steepened valley flanks after the retreat of the glaciers, partly triggered by earthquakes (Radbruch-Hall 1978; Gutiérrez-Santolalla et al. 2005). In contrast, Jarman (2006) argues for an additional influence of postglacial rebound. His speculation would be supported by our findings.

Conclusion

Field observations and numerical experiments show that faults with uphill-facing scarps develop only in valleys with steeply dipping lithologic boundaries or schistosity. Three processes, which may have different relative importance depending on the local setting, are responsible for their formation: postglacial differential uplift (as shown by numerical modelling), gravitational slope movements (as deduced from field observations) and tectonics (suggested to be a consequence of the tectonic setting). In the Swiss Alps, where uphill-facing scarps occur in formerly glaciated regions, differential uplift during deglaciation triggered slip on the pre-existing weak zones. Considerable slip was accumulated by subsequent gravitational slope movements and, in some places, by tectonic displacement. Composite faults may be distinguished from tectonic faults by their orientation parallel to the valley axis and their large along-strike variations in displacement. In contrast to composite faults, tectonic faults usually can be traced across several valleys. Our results imply that attempts to decipher the current tectonic deformation pattern in an orogen must take into account that faults scarps may not always be of tectonic origin but that gravitational slope movements and postglacial differential uplift may have produced or modified the scarps.

Acknowledgements

This work was financially supported by the Canton of Bern, the Swiss National Science Foundation (grant no. 2000-067952) and the Swiss Geophysical Commission (project: Swiss Seismotectonic Atlas), for which we are much obliged. Funding to A.H. by the German Research Foundation (DFG) within the framework of the Emmy-Noether-Program (grant no. HA 3473/2-1) is gratefully acknowledged. We thank Susan Ellis and Jean-Claude Hippolyte for their critical and constructive reviews, which helped improving the manuscript.

REFERENCES

Adams, J. 1989: Postglacial faulting in eastern Canada: Nature, origin, and seismic hazard implications, Tectonophysics 163, 323–331.

Agliardi, F., Crosta, G. & Zanchi, A. 2001: Structural constraints on deep-seated slope deformation kinematics. Engineering Geology 59, 83–102.

Amann, F. 2005: Großhangbewegung Cuolm Da Vi (Graubünden, Schweiz): Geologisch-geotechnische Befunde und numerische Untersuchungen zur Klärung des Phänomens. PhD Thesis, Friedrich-Alexander-Universität Erlangen-Nürnberg, Erlangen, 207 pp.

Arvidsson, R. 1996: Fennoscandian earthquakes: whole crustal rupturing related to postglacial rebound. Science 274, 744–746.

Bachmann, D., Bouissou, S. & Chemenda, A. 2004: Influence of weathering and pre-existing large scale fractures on gravitational slope failure: insights from 3-D physical modelling. Natural Hazards and Earth System Sciences 4, 711–717.

Baer, M., Deichmann, N., Fäh, D, Kradolfer, U., Mayer-Rosa, D., Rüttener, E., Schler, T., Sellami, S. & Smit, P. 1997: Earthquakes in Switzerland and surrounding regions during 1996. Eclogae Geologicae Helvetiae 90, 557–567.

Barletta, V.R., Ferrari, C., Diolaiuti, G., Carnielli, T., Sabadini, R. & Smiraglia, C. 2006: Glacier shrinkage and modeled uplift of the Alps. Geophysical Research Letters 33, L14307, doi:10.1029/2006GL026490.

Benn, D.I. & Evans, D.J.A. 1998: Glaciers and glaciation. Arnold, London, 734 pp.

Bilham, R., Larson, K. & Freymueller, J. 1997: GPS measurements of present-day convergence across the Nepal Himalaya, Nature 386, 61–64.

Bovis, M.J. 1982: Uphill-facing (antislope) scarps in the Coast Mountains, southwest British Columbia. Geological Society of America Bulletin 93, 804–812.

Brückl, E. & Parotidis, M. 2005: Prediction of slope instabilities due to deep-seated gravitational creep. Natural Hazards and Earth System Sciences 5, 155–172.

Deichmann, N., Baer, M., Braunmiller, J., Cornou, C., Fäh, D., Giardini, D., Gisler, M., Huber, S., Husen, S., Kästli, P., Kradolfer, U., Mai, M., Maraini, S., Oprsal, I., Schler, T., Schorlemmer, D., Wiemer, S., Wössner, J. & Wyss, A. 2004: Earthquakes in Switzerland and surrounding regions during 2003. Eclogae Geologicae Helvetiae 97, 447–458.

Deichmann, N., Baer, M., Braunmiller, J., Husen, S., Fäh, D., Giardini, D., Kästli, P., Kradolfer, U. & Wiemer, S. 2006: Earthquakes in Switzerland and surrounding regions during 2005. Eclogae Geologicae Helvetiae 99, 443–452.

Dramis, F. & Sorriso-Valvo, M. 1994: Deep-seated gravitational slope deformations, related landslides and tectonics. Engineering Geology 38, 231–243.

Eckardt, P., Funk, H. & Labhart, T. 1983: Postglaziale Krustenbewegungen an der Rhein-Rhone-Linie. Mensuration, Photogrammétrie, Génie rural 2, 43–56.

Flageollet, J.-C. 1989: Les Mouvements de Terrain et leur Prévention. Masson, Paris, 221 pp.

Florineth, D. & Schlüchter, C. 1998: Reconstructing the Last Glacial Maximum (LGM) ice surface geometry and flowlines in the Central Swiss Alps. Eclogae Geologicae Helvetiae 91, 391–401.

Furrer, H. 1948: Das Sackungsgebiet von Greich-Goppisberg, nördlich Mörel, und der Rinderhornstollen (Oberwallis). Eclogae Geologicae Helvetiae 41, 291–296.

Gudmundsson, G.H. 1994: An order-of-magnitude estimate of the current uplift-rates in Switzerland caused by the Wurm Alpine deglaciation. Eclogae Geologicae Helvetiae 87, 545–557.

Gutiérrez-Santolalla, F., Acosta, E., Rios, S., Guerrero, J. & Lucha, P. 2005: Geomorphology and geochronology of sackung features (uphill-facing scarps) in the Central Spanish Pyrenees. Geomorphology 69, 298–314.

Hampel, A. & Hetzel, R. 2006: Response of normal faults to glacial-interglacial fluctuations of ice and water masses on Earth's surface. Journal of Geophysical Research 111, B06406, doi:10.1029/2005JB004124.

Hetzel R., Tao, M., Stokes S., Niedermann S., Ivy-Ochs S., Bo G., Strecker M.R. & Kubik P.W. 2004: Late Pleistocene/Holocene slip rate of the Zhangye thrust (Qilian Shan, China) and implications for the active growth of the northeastern Tibetan Plateau, Tectonics 23, TC6006, doi:10.1029/2004TC001653.

Hetzel, R. & Hampel, A. 2005: Slip rate variations on normal faults during glacial-interglacial changes in surface loads. Nature 435, 81–84. doi: 10.1038/nature 03562.

Hibbitt, Karlson & Sorenson 2006: ABAQUS/Standard version 6.6, Hibbitt, Karlson and Sorenson Inc., Pawtucket, RI, USA.

Hippolyte, J.-C., Brocard, G., Tardy, M., Nicoud, G., Bourlès, D., Braucher, R., Ménard, G. & Souffaché, B. 2006: The recent fault scarps of the Western Alps (France): Tectonic surface ruptures or gravitational sackung scarps? A combined mapping, geomorphic, levelling, and 10Be dating approach. Tectonophysics 418, 255–276.

Hoek, E. & Bray, J.W. 1981: Rock slope engineering. 3rd edition, The Institution of Mining and Metallurgy, London, England, 360 pp.

Ivy-Ochs, S., Kerschner, H., Reuther, A., Maisch, M., Sailer, R., Schaefer, J., Kubik, P.W., Synal, H.-A. & Schlüchter, C. 2006: The timing of glacier advances in the northern European Alps based on surface exposure dating with cosmogenic ^{10}Be, ^{26}Al, ^{36}Cl and ^{21}Ne. Geological Society of America Special Paper 415, 43–60.

Jäckli, H. 1951: Verwerfungen jungquartären Alters im südlichen Aarmassiv bei Somvix-Rabius (Graubünden). Eclogae Geologicae Helvetiae 44, 332–337.

Jäckli, H.C.A. 1965: Pleistocene glaciation of the Swiss Alps and signs of postglacial differential uplift. The Geological Society of America, Special paper 84, 153–157.

Jarman, D. 2006: Large rock slope failures in the Highlands of Scotland: Characterisation, causes and spatial distribution. Engineering Geology 83, 161–182.

Johnston, P., Wu, P. & Lambeck, K. 1998: Dependence of horizontal stress magnitude on load dimension in glacial rebound models. Geophysical Journal International 132, 41–60.

Jomard, H. 2006: Analyse mulit-échelles des deformations gravitaires du Massif de l'Argentera Mercantour. PhD Thesis, Université de Nice Sophia-Antipolis, Nice, 254 pp.

Kahle, H.-G., Geiger, B., Bürki, B., Gubler, E., Marti, U., Wirth, M., Rothacher, M., Gurtner, W., Beutler, G., Bauersima, I. & Pfiffner, O.A. 1997: Recent crustal movements, geoid and density distribution: Contribution from integrated satellite and terrestrial measurements. In: Pfiffner, O.A., Lehner, P., Heitzmann, P., Müller, St. & Steck, A. (Eds.): Deep Structure of the Swiss Alps: Results of NRP 20. Birkhäuser, Basel, pp. 251–259.

Kammer, A. 1985: Bau und Struktur des nördlichen Aarmassivs und seine Sedimente zwischen dem Sustenpass und Grindelwald (Berner Oberland). PhD Thesis. Université de Neuchâtel, Neuchâtel, 110 pp.

Keller, F. & Schneider, T.R. 1982: Geologie und Geotechnik, Der Furka-Basistunnel: Zur Eröffnung am 25. Juni 1982, Schweizer Ingenieur und Architekt 100, 512–520.

Kelly, M., Buoncristiani, J.-F. & Schlüchter, C. 2004: A reconstruction of the last glacial maximum (LGM) ice-surface geometry in the western Swiss Alps and contiguous Alpine regions in Italy and France. Eclogae Geologicae Helvetiae 97, 57–75.

Kelly, M.A., S. Ivy-Ochs, Kubik, P., Von Blanckenburg, F.W. & Schlüchter, C. 2006: Chronology of deglaciation based on ^{10}Be dates of glacial erosional features in the Grimsel Pass region, central Swiss Alps. Boreas 35, 634–643.

Madritsch, H. & Millen, B.M.J. 2007: Hydrogeologic evidence for a continuous basal shear zone within a deep-seated gravitational slope deformation (Eastern Alps, Tyrol, Austria). Landslides 4, 149–162, doi 10.1007/s10346-006-0072-x.

Mahr, T. & Nemcok, A. 1977: Deep-seated creep deformations in the crystalline cores of the Tatry Mts. Bulletin of the International Association of Engineering Geology 16, 104–106.

McCalpin, J.P. & Irvine J.R., 1995: Sackungen at the Aspen Highlands Ski area, Pitkin County, Colorado. Environmental and Engineering Geoscience 1, 277–290.

Molnar, P. & Tapponnier, P. 1975: Cenozoic tectonics of Asia: Effects of a continental collision. Science 189, 419–426.

Persaud, M. & Pfiffner, O.A. 2004: Active deformation in the eastern Swiss Alps: post-glacial faults, seismicity and surface uplift. Tectonophysics 385, 59–84.

Preusser, F. 2004: Towards a chronology of the Late Pleistocene in the northern Alpine Foreland. Boreas 33, 195–210.

Radbruch-Hall, D.H. 1978: Gravitational creep of rock masses on slopes. In: B. Voight (Editor), Rockslides and Avalanches, 1 – Natural Phenomena. Developments in Geotechnical Engineering. Elsevier, Amsterdam, Oxford, New York, pp. 607–657 (Chapter 17).

Renner, F. 1982: Beiträge zur Gletschergeschichte des Gotthardgebietes und dendrochronologische Analysen an fossilen Hölzern. Physische Geographie 8. Furrer, Keller, Gamper, Suter, Zürich, 180 pp.

Sartori, M., Bailifard, F., Jabeyedoff, M. & Rouiller, J.-D. 2003: Kinematics of the 1991 Randa rockslides (Valais, Switzerland). Natural Hazards and Earth System Sciences 3, 423–433.

Sauber, J., Plafker, G., Molnia, B.F. & Bryant, M.A. 2000: Crustal deformation associated with glacial fluctuations in the eastern Chugach Mountains, Alaska. Journal of Geophysical Research 105, 8055–8077.

Schmid, S.M., Pfiffner, O.A., Froitzheim, N., Schönborn, G. & Kissling, E. 1996: Geophysical-geological transect and tectonic evolution of the Swiss-Italian Alps. Tectonics 15, 1036–1064.

Selzer, C. 2006: Tectonic accretion styles at convergent margins: A numerical modelling study. PhD Thesis, University of Bern, Bern, 97 pp.

Selzer, C., Buiter, S.J.H. & Pfiffner, O.A. 2008: Numerical modelling of frontal and basal accretion at convergent margins. Tectonics, doi: 10.1029/2007 TC 002169, in press.

Stewart, I.S., Sauber, J. & Rsoe, J. 2000: Glacio-seismotectonics: ice sheets, crustal deformation and seismicity. Quaternary Science Reviews 19, 1367–1389.

Tapponnier, P. & Molnar, P. 1979: Active faulting and Cenozoic tectonics of the Tien Shan, Mongolian, and Baykal regions. Journal of Geophysical Research 84, 3425–3459.

Turcotte, D.L. & Schubert G. 2002: Geodynamics. Cambridge University Press, 2nd edition, 456 pp.

Twiss, R.J. & Moores, E.M. 2007: Structural Geology. 2nd edition, W.H. Freeman and Co., New York, 736 pp.

Ustaszewski, M. 2007: Neotectonics in the central and western Swiss Alps. Ph.D. thesis, University of Bern.

Ustaszewski, M. & Pfiffner, O.A. (2008): Neotectonic faulting, uplift and seismicity in the central and western Swiss Alps. In: Siegesmund, S. Fügenschuh, B. & Froitzheim, N. (Eds.): Tectonic Aspects of the Alpine-Dinaride-Carpathian System. Geological Society, London, Special Publication, 298, 231–249.

Wang, Q., P.-Z. Zhang, J.T. Freymueller, R. Bilham, K.M. Larson, X. Lai. X. You, Z. Niu, J. Wu, Y. Li, J. Liu, Z. Yang & Q. Chen 2001: Present-day crustal deformation in China constrained by Global Positioning measurements. Science 294, 574 -577.2001. Present-day crustal deformation in China constrained by Global Positioning measurements. Science 294, 574–577.

Weijermars, R. 1997: Principles of Rock Mechanics, Alboran Science Publishing, Netherlands, 360 pp.

Van der Woerd, J., Xiwei, X., Haibing, L., Tapponnier, P., Meyer, B., Ryerson, F.J., Meriaux, A.-S. & Zhiqin, X. 2001: Rapid active thrusting along the northwestern range front of the Tanghe Nan Shan (western Gansu, China). Journal of Geophysical Research 106, 30,475–30,504.

Manuscript received April 4, 2007
Revision accepted July 7, 2007
Published Online first April 4, 2008
Editorial Handling: Stefan Bucher